



**Molecular Design Confirmation for Proposition of Improved
Photophysical Properties in a Dye-Intercalated Layered
Double Hydroxides**

Journal:	<i>RSC Advances</i>
Manuscript ID	RA-ART-09-2015-019209.R2
Article Type:	Paper
Date Submitted by the Author:	15-Jan-2016
Complete List of Authors:	Arjomandi Rad, Farzad; Azarbaijan Shahid Madani University, Chemistry Rezvani, Zolfaghar; Azarbaijan Shahid Madani University, Chemistry Khodam, Fatemeh; Azarbaijan Shahid Madani University, Chemistry
Subject area & keyword:	Optical materials < Materials



ARTICLE

Molecular Design Confirmation for Proposition of Improved Photophysical Properties in a Dye-Intercalated Layered Double Hydroxides

Received 00th January 20xx,
Accepted 00th January 20xx

DOI: 10.1039/x0xx00000x

www.rsc.org/

Farzad Arjomandi Rad, Zolfaghar Rezvani*, and Fatemeh Khodama

Abstract:

In the present research, Zn₂Al layered-double hydroxide (LDH) intercalated with Acid Red 27 was prepared by coprecipitation method, while solutions of Zn(II) and Al(III) nitrate salts reacted with an alkaline solution of Acid Red27. Successful intercalation of the Acid Red 27 molecules into the interlayer space of LDH was confirmed by powder X-ray diffraction, FTIR spectroscopy, and thermal gravimetric analysis (TGA). The photoluminescence (PL) analysis and diffuse reflectance spectroscopy (DRS) were investigated and correlated with fluorescent property and photocatalytic capability of the Red 27- Zn₂Al-LDHs system. The interlayer structure, nonbonding forces, and *H-type* (face-to-face arrangement) aggregates of the Acid Red 27 molecules in the interlayer space of the Zn₂Al-LDH layers were studied by the molecular dynamic simulation. Geometry optimization, the radial distribution function (RDF), mean square displacement (MSD), and angle distribution of the Acid Red 27 molecules were calculated using the trajectory files on the basis of the molecular dynamic (MD) simulations. Good agreement between the calculated and measured X-ray diffraction patterns was obtained. The MD results indicated that the Acid Red 27 molecules were more immobilize when aggregated with coplanar conformation and intercalated into the LDH layers. The aggregation-induced emission improvement of the Red 27- Zn₂Al-LDHs system was studied for predicating the effective photofunctional properties of Red 27- Zn₂Al-LDHs.

Keywords: Red 27-Zn₂Al-LDH, Molecular dynamic simulation, Photoluminescence, H-type aggregation

^a Department of Chemistry, Faculty of Basic Sciences, Azarbaijan Shahid Madani University, Tabriz, Iran, Fax: +98 412 432 7541; Tel: +98 412 432 7541; E-mail: zrezvani@azaruniv.ac.ir



ARTICLE

1. Introduction

Azo dyes have attracted significant attention due to their multi-purpose applications in various areas. Their position in dye industry, biological chemistry, and many high technologies has been reported formerly.¹⁻⁴ Organic dyes have been used as the capable candidates for various nonlinear optical (NLO) applications such as luminescent efficiency because of the delocalization behavior of their electrons, which gives rise to large optical nonlinearities.⁵ Such optical properties influenced the spectroscopic properties of the molecules and also were influenced by their crystallographic arrangements.^{6,7} The side groups around the azo bond support stabilizing the N=N group by constructing it as part of an extensive delocalized system. Azo dyes act as the electron acceptors.⁸ The sulfonated and carboxylated azo dyes, mainly mono, di, and tri sulfonated compounds, are globally allowed to be used as the colorant in foods, cosmetics, and drugs for oral uses.^{9,10} Various azo compounds have been intercalated into the gallery field of LDHs, e.g. o-methyl red (MR)¹¹ [2-(4-(dimethyl-amino) phenylazo) benzoic acid], C.I. Mordant Yellow 10 [2-hydroxy-5-(4-sulfophenyl azo) - benzoate] disodium salt,¹² C.I. Pigment Red 52:1,¹³ C.I. Pigment Red 48:2,¹⁴ blue black (NBB),¹⁵ and 7- phenoxy-pentanoate anion (CF₃AZO).¹⁶

Layered double hydroxides (LDHs) are a typical two-dimensional (2D) host matrix which can be described by the general formula of $M^{II}_{1-x}M^{III}_x(OH)_2A^{n-}_{x/n} \cdot mH_2O$, where M^{II} and M^{III} are the divalent and trivalent metals, respectively, and Aⁿ⁻ is an anion. The positively-charged host layers are electrically balanced by the anions in the interlayer space,¹⁷ and the efficient anions can be assembled within LDHs for creating new types of organic-inorganic hybrid materials.¹⁸ There has been considerable attention to many organic anions with the acidic head group including carboxylates, sulfonates, benzoates, and biomolecular anions such as azo dyes, aminoacides, enzymes, and drugs incorporated in LDHs.¹⁹ These materials are a class of 2D inorganic layered matrices²⁰⁻²³ which have been widely used in

photocatalysis,^{24,25} dye-sensitized solar cells,²⁶ adsorption,²⁷ CO₂ adsorbents,^{28,29} and functional materials.^{30,31} Hydrotalcite-like compounds can be prepared by various techniques. The most common method is coprecipitation, in which solutions of M^{II} and M^{III} salts react with an alkaline solution. The coprecipitated products containing easily replaceable anions (e.g., NO₃⁻ or Cl⁻) are commonly used as the precursors in the anion exchange reactions. Flexibility in chemical composition and physical-chemical properties of the hydrotalcite-like compounds suggest a great variety in the use of these materials, e.g. in heterogeneous catalysis, adsorption and decontamination processes, polymer processing, and preparation of the new inorganic/organic hybrid materials.³²⁻³⁴

Recent assembly of the organic azo dye molecules incorporated into the inorganic host matrices³⁵ has received significant attention due to the following advantages: firstly, the orderly distribution and arrangement of the dye molecules within the regular framework is favorable for the improvement of the luminescent efficiency of the organic-inorganic hybrid materials, which is a requirement for fabricating a new generation of the solid-state dye laser and dye-based molecular optical devices.³⁶ Secondly, the solid matrices can offer higher mechanical, thermal, and chemical stability for the dye molecules.³⁷ Thirdly, the LDH monolayers have the ability to avoid interpenetration between the adjacent layers, which often occurs in polymer films.³⁸ And last but not least, the LDH interlayer channels are easier to be penetrated, facilitating the realization of the optical/chemical sensors with rapid responding and recyclability.³⁹ By the use of co-precipitation method, the single-component chromophore molecules can be intercalated into the LDH galleries. It was found that intercalation into LDH has weakened the strong π - π interaction between the anions, which has paved the way for their application in solid-state optoelectronic devices with high performance. Also layer-by-layer (LbL) assembly is a broadly used method to achieve multilayer LDH-based ultrathin films (UTFs),

which involves alternative dipping of a substrate in positively charged LDH nanosheets and negatively charged photofunctional molecules.⁴⁰

Recently, Yan et al have fabricated a new type of piezochromic luminescence (PCL) material by the assembly of an organic anion (BTZB) into the nanogalleries of LDHs. Upon increasing pressure, BTZB/LDH nanocomposites exhibit luminescent red shift with a simultaneous broadening of the emission, while the pristine BTZB shows no PCL at all.⁴¹

Moreover, Yan et al have reported a mechano-induced and solvent stimuli-responsive luminescent change by the assembly of a typical aggregation induced-emissive (AIE) molecule, niflumic acid (NFC), into the interlayer region of Zn-Al layered double hydroxides (LDHs) with heptane sulfonate (HPS) as the co-intercalation guest.⁴² They have also reported transparent and flexible thin films based on alternate layer-by-layer assembly of sulfonated Eu- and Tb-based lanthanide complexes (LCs) and Mg-Al-layered double hydroxide (LDH) nanosheets with UV-visible absorption and enhanced fluorescence property.⁴³ Furthermore, they have reported the layer-by-layer co-assembly of two types of two-color (blue/red) luminescent ultrathin films (UTFs) by using different photofunctional anions and Mg-Al-layered double hydroxide (LDH) nanosheets as the basic building blocks with well-defined two-color polarized fluorescence.⁴⁴

In another research work by Yan et al, a new type of host-guest UV-blocking material with higher photoluminescence quantum yield has been synthesized by the introduction of a fluorescent anion, 2-[2-[4-[2-(4-carboxyphenyl)vinyl]phenyl]-vinyl]benzoate (CPBA), into the interlayer galleries of a Zn-Al-NO₃ layered double hydroxide (LDH) precursor using an anion-exchange method.⁴⁵ Finally, they have fabricated (CXT/LDH)nTFs by a layer-by-layer assembly technique, which shows well-defined blue photoluminescence. Moreover, the TFs display a fast luminescence response as the colorimetric chemosensor for the sensing applications.⁴⁶ Recently some researchers have reported that the organic dye anions/ LDH systems exhibit blue-shift photoemission and enhanced fluorescence efficiency compared with those of the pristine azo dye sample, and the Azo dye/ LDH thin films exhibit precise polarized luminescence with the fluorescence anisotropy characterization.

Newman et al⁴⁷ investigated the interlayer structure of an Mg₃Al-LDH model containing amino acids. The combination methods will become a major development in the near future. The simulations

offer detailed insight into the arrangement of the counter ions and water molecules in the interlayer, but the results were not generally available from the experiment. These simulations provided a powerful technique to analyze the structure as well as the dynamic properties at the molecular level, and it also provided a direct connection between the local structural details and the experimental measurements. So in the recent years, there have been many researchers who used a mixture of theoretical and experimental methods to study the same system and have obtained great achievements.^{48,49} Yuan et al⁵⁰ studied intercalation of the photoactive dyes into layered double hydroxides by the molecular dynamic simulation. The results indicated that the photoactive dyes intercalated into the LDH structures can possibly be applied in the field of optoelectronic and photonic materials, and the results obtained from the hybrid-LDH materials could be used to enhance understanding the structure of the other hybrid-LDHs intercalated with more complex anion structures.⁵⁰

In our previous work, we prepared Mg-Al hydrotalcite intercalated by cubane-dc anions and then studied the distribution of the cubane-dc anions at the molecular level by the molecular dynamic (MD) study. The aforementioned distribution resulted from non-bonding and the host-guest interactions based on van der Waals and electrostatic forces in cubane-dc-Mg-Al-LDH.⁵¹ In this work, intercalation of Acid Red 27 into the Zn-Al-LDH host was carried out through the co-precipitation method using the zinc and aluminum salts and pristine dye. The product was obtained by the coprecipitation method when solutions of the M(II) and M(III) salts react with an alkaline solution of Acid Red 27. Experimental analysis of the acid Red 27-LDH using FT-IR and X-ray diffraction confirmed the intercalation process, and TGA approved thermostability of the synthesized acid Red 27-LDH. The size and morphology of these materials were studied by scanning electron microscopy (SEM). Since the physicochemical properties of the intercalates are influenced by the structure of the interlayer space, the molecular modeling was used to describe the arrangement of the Acid Red 27 molecules in the interlayer space. The photoluminescence (PL) spectroscopy was used for investigating the optical properties attributed to the host-guest interactions in the LDH nanohybrids, and the diffuse reflectance spectroscopy (DRS) was carried out for studying the electronic structure of the azo dye-LDH system. We simulated the arrangement of the interlayer space of Red 27-LDH and focused on the microscopic position and dynamic properties of

the intercalated molecules. The simulation results are in reasonable agreement with the experimental results and are favorable tools for prediction of the fluorescent efficiency enhancement compared with that of the pristine azo dye sample through parallel (face to face) aggregation of the Acid Red 27 molecules in Zn:Al-LDH as the opto-functional materials.

2. Experimental

2.1 Materials

Acid Red 27 or amaranth, a mono azo anionic dye, was obtained from Merck Co., the chemical formula of which is $C_{20}H_{11}N_2Na_3O_{10}S_3$ with the 120 °C melting point. All of the reagents were purchased from Merck chemical company and used without further purification.

2.2 Syntheses of Red 27–Zn₂Al–LDH

A solution containing Acid Red 27 (0.6044 g, 0.001 mol) dissolved in NaOH (20 mL, 0.1 M) was slowly added to an aqueous mixed solution (20 mL) of $Zn(NO_3)_2 \cdot 6H_2O$ (0.5949 g, 0.002 mol) and $Al(NO_3)_3 \cdot 9H_2O$ (0.375 g, 0.001 mol) under vigorous stirring in the nitrogen atmosphere. The pH of the solution was adjusted to 10 by dropwise adding of NaOH or HCl. The system was heated to reflux at 70 °C for 72h for intercalation of the Red 27 anions into NO_3 -LDH. The product (Red 27–LDH) was centrifuged at the speed of 2000 rpm for 10 min and the solid was washed thoroughly with deionized water and finally dried at room temperature in vacuum. Anal. Calculated for $[Zn_4Al_2(OH)_{12}](C_{20}H_{11}N_2O_{10}S_3)_{0.66} \cdot 4.5H_2O$: C, 16.70; H, 2.95; N, 1.94; Zn, 27.31; Al, 5.64. Found: C, 16.3; H, 2.7; Zn, 27.1; Al, 5.2.

2.3 Characterizations

Powder X-ray diffraction patterns (PXRD) of the samples were recorded with a Bruker AXS model D8 Advance Diffractometer using $Cu-K\alpha$ radiation ($\lambda = 1.54 \text{ \AA}$) at 40 kV, 35 mA with a Bragg angle ranging from 3 to 70° 2 θ . Fourier transform infrared spectra (FT-IR) were recorded in the range of 4000–400 cm^{-1} using the KBr pellet technique with a Perkin-Elmer spectrophotometer. TGA was carried out with a Mettler-Toledo TGA 851e apparatus at the heating rate of 10 $Kmin^{-1}$ in the nitrogen atmosphere. The scanning electron microscopy (SEM) was used to study the morphology of the samples and the SEM analysis was performed for the Au-coated samples using a Philips apparatus model XL30. Zn and Al contents of

the samples were determined using inductively coupled plasma spectroscopy (Jobin Yvon JY24) after dissolving the samples in nitric acid. Elemental (C, H, and N) analyses were carried out on a Perkin-Elmer 240B analyzer. Diffuse reflectance spectroscopy (DRS) was recorded with the wavelength monitoring method by absorbance ranging from 200 nm to 1000 nm (Firmware Version: 061020 Software Version: LabProPlus Build 410.1). The photoluminescence emission spectra of the samples were recorded using a JASCO luminescence spectrometer with the excitation wavelength of 260 nm and 240 nm.

2.4 Methods for molecular modeling

The whole simulations were conducted using the Discover and Forcite modules in the Materials Studio software package.⁵² These modules involve a range of well-validated force fields for dynamic simulations, minimization, and analysis searches for the periodic solids. They can be desirably employed in studying the molecular system and crystalline materials. A perfect LDH layer model with the hexagonal supercell was made in this research. At first, the DFT method was used to get the geometrically optimized configuration for Acid Red 27. After determination of the atomic charges, this information would be used in the molecular dynamic simulations. The *Dreiding* classical force field was used for the system.^{47, 53}

The first step in arranging models of intercalates was construction of the host positively charged layers. The hydroxide layers of $Zn_4Al_2(OH)_{12}CO_3 \cdot 3H_2O$ were built using the atomic coordinates from the previously reported crystal structure of the hydroxalcite. The host was a three-layered structure which included a rhombohedral lattice with hexagonal unit-cell parameters of $a_b = 3.06616 \text{ \AA}$, $c = 22.6164 \text{ \AA}$, $\alpha = \beta = 90^\circ$, and $\gamma = 120^\circ$ ⁵⁴ and the space group was $R\bar{3}m$. In order to study the mutual arrangement of the guests in the interlayer space, a $P1$ superlattice with the dimensions of $6a \times 3a \times 3d_{exp}$ was established where d_{exp} was obtained from the X-ray diffraction data of Red 27-LDH. The interlamellar carbonate ions and water molecules were omitted, then a supercell was developed in $6a \times 3b \times 2.25c$ with lattice parameters of $6a = 18.39696 \text{ \AA}$, $3b = 9.19848 \text{ \AA}$, and $2.25c = 50.952 \text{ \AA}$, where $d_{exp} = 16.984 \text{ \AA}$, and the ratio of Zn/Al atoms in the framework was 2:1, and the Zn and Al atoms were scattered in every layer arbitrarily. Every hydroxide layer had $6Al^{3+}$ and $12Zn^{2+}$ ions, with the former arranged in a way that they were not placed in the adjacent octahedrals. The Red 27 anions were randomly located in the interlamellar area of LDH to

neutralize the positive charges of the hybrid system, and then to form a tilted bilayer organization. The molecules of water (14 molecules) were also randomly inserted into the interlamellar space. The atomic charges are obtained from the Mulliken charge, APT charge, and ESP charge.

In this work, the ESP (electrostatic potential) method⁵⁵ was used for calculation of the atomic charges. Fig. 1 shows the ESP charge of Acid Red 27 as the non-planar organic molecule. The Dmol₃ program at the GGA-PBE/DND level optimized the Acid Red 27 structure. The atomic charges are essential in explaining the Acid Red 27 structure and the MD properties when the Acid Red 27 anions were placed into the LDH layer.

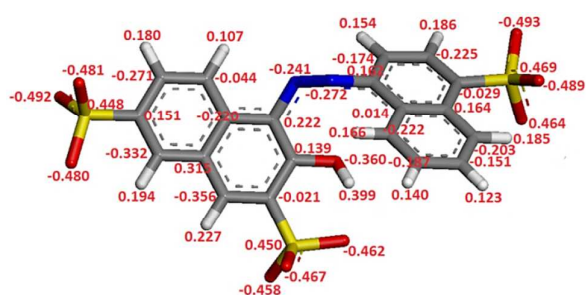


Fig. 1 The ESP atomic charges of Acid Red 27 as a non-planar organic molecule

The layer charges were calculated, using the charge equilibration (QEq) method. Since the Dreiding force field is acceptable for Zn₂Al-LDHs,⁴⁸ the charges of the LDH layers were improved with regard to the Dreiding force field, and the partial charge for Al was set to 1.458e or 1.586e, for Zn to 0.316e or 0.427e, for O to -0.480e or -0.535e, and for H to 0.239e or 0.344e. The calculated partial charge of the oxygen and hydrogen atoms of the layers increased in comparison with our previous work,⁵¹ in which we studied cubane-1,4-dicarboxylate-intercalated Mg₂Al-LDH. This indicates that Acid Red 27 as an intercalated anion has strong nonbonding interaction with the layers, compared to our previous work.⁵¹

The minimization was performed in Dreiding force field. The electrostatic energy was found by the Ewald summation method,⁵⁶ and the van der Waals energy was shown by the Lennard–Jones potential.⁵⁷ The total crystal energy minimization was conducted by the smart minimizer method considering the following approach: all of the layers of the host were kept as the firm units in the energy minimization period, and the cell parameters *c*, *a*, and *b* were variable. It enabled optimization of the mutual arrangement of the

host layers. All the atomic positions in the interlayer region were variable too. In this research, we concentrated on the aggregation structure of the molecules of Acid Red 27 intercalated into LDH. The simulation started from the structures with minimized energy, and the smart minimizer procedure was employed for minimization. The minimized structure was employed to set the equilibrium bond lengths and angles. The molecular dynamic simulation was carried out in the NPT statistical ensemble at room temperature (298 K). The time step was 0.4 fs and the total time of simulation was 2000 ps. Fig. S1 in the Supporting Information shows that the potential energy profile reaches stable equilibrium after about 1000 ps of simulation time and the last 2000 ps was used for further analysis.

3. Results and Discussion

3.1 The Structural Characterizations of Zn₂Al–NO₃–LDHs

Fig. 2 shows the XRD pattern of Zn₂Al–NO₃–LDHs and Red 27-LDH and their characteristic reflections related to the crystalline layered phase.⁵⁸ In the range of 2-70° for Zn₂Al–NO₃–LDHs, the sharp and strong diffraction peaks at the low 2θ values, shown in Fig. 2a, demonstrate good crystallinity of the LDH nanoparticles.

Zn₂Al–NO₃–LDHs have *d*₀₀₃ basal spacing of 8.73 Å. This spacing, which represents summation of the thickness of the brucite-like layer (0.48 nm)⁵⁹ and the gallery height, is a function of the number, size, and orientation of the intercalated anions.⁶⁰ The XRD pattern of the sample with the intercalated Red 27 anion is shown in Fig. 2 b. During intercalation of the Acid Red 27 molecules, the layers of LDH swell to host the anions and this expansion is reflected by the 16.98 Å value of its *d*₀₀₃. This swelling of the layers is due to intercalation of the Acid Red 27 molecules and the basal spacing corresponding to the diffraction by the (003) plane is much larger than that of LDH. Taking into account that the thickness of the LDH layer is 4.8 Å and the longitudinal van der Waals radius of the Red 27 anion is 15.432 Å, it was confirmed that the Acid Red 27 molecules were successfully intercalated with horizontally slanted (The width of the Acid Red 27 molecule is equal to 9.842 Å) orientation in their anionic form, and that they were arranged with sufficient space as a monolayer within the interlayer.

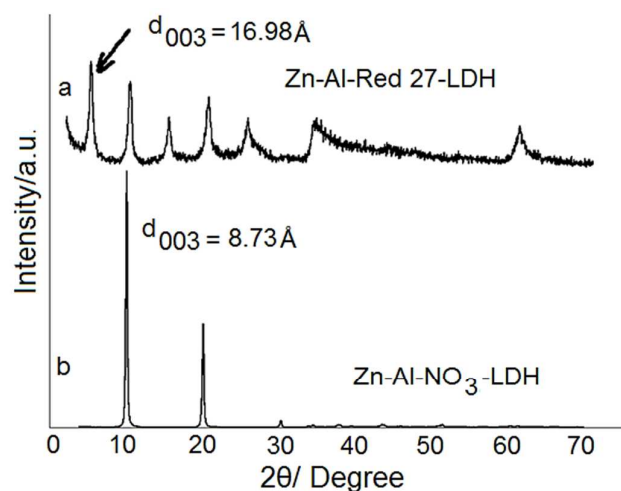


Fig. 2 PXRD patterns of the $\text{Zn}_2\text{Al-NO}_3\text{-LDH}$ precursor and $\text{Zn}_2\text{Al-LDH}$ intercalated with Acid Red 27

The structure of Red 27- $\text{Zn}_2\text{Al-LDH}$ was also confirmed by the FT-IR spectroscopy. The FT-IR spectra of Red 27- $\text{Zn}_2\text{Al-LDH}$, $\text{NO}_3\text{-Zn}_2\text{Al-LDH}$, and Acid Red 27 are shown in Fig. 3 a–c, respectively.

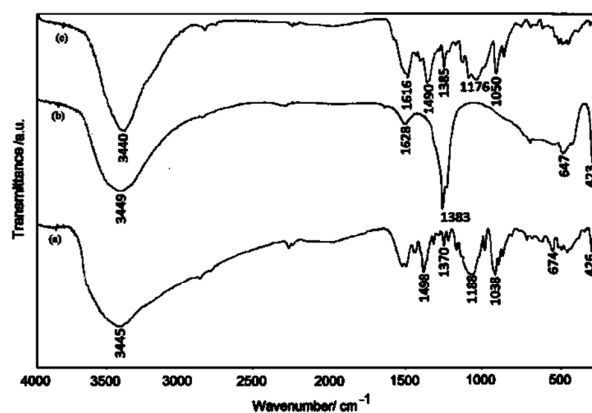


Fig. 3 FT-IR spectra of a) Red 27- $\text{Zn}_2\text{Al-LDH}$, b) $\text{NO}_3\text{-Zn}_2\text{Al-LDH}$, and c) Acid Red 27

The spectrum of $\text{NO}_3\text{-Zn}_2\text{Al-LDH}$ is similar to that reported in the literature.^{61,62} Absorption at 1383 cm^{-1} can be assigned to the ν_3 vibration of NO_3 . The broad strong absorption band centered at 3449 cm^{-1} is ascribed to the stretching vibrations of the hydroxyl groups and the surface and interlayer water molecules,^{63,64} which are found at a lower frequency in LDHs compared with the O–H stretching in free water at 3600 cm^{-1} .⁶⁵ This is attributed to the formation of the hydrogen bonds between the interlayer water molecules and the different guest anions as well as with the hydroxide groups of the layers. The weaker band at 1628 cm^{-1} was

due to the bending mode of the water molecules. The bands centered at 423 and 647 cm^{-1} are attributed to the Al–O and Zn–O lattice vibrations.⁶¹ These values reduced in comparison with 446 and 672 cm^{-1} values attributed to Al–O and Mg–O lattice vibrations in our previous work.⁵¹

In the case of pure Acid Red 27, the strong absorption band at 3440.40 cm^{-1} is attributed to the stretching vibrations of the OH groups. Furthermore, the absorption band at 1490 cm^{-1} is related to the C=C groups of the aromatic rings which were conjugated to the nitrogen atoms of the azo system and connected to the sulfonate groups. The absorption bands at 1050 cm^{-1} and 1176 cm^{-1} correspond to the S=O symmetric and asymmetric stretching vibrations of the sulfonate groups and the absorption band at 1616 cm^{-1} is attributed to the N=N stretching vibrations of the azo group.⁶⁶ After intercalation of the Acid Red 27 molecules, the absence of the NO_3 bands at 1383 cm^{-1} in the spectrum of the exchanged LDH indicates that the exchange process was complete. The bands at 1050 cm^{-1} and 1176 cm^{-1} disappear due to the symmetric and asymmetric stretching vibrations of the free SO_3^- group, while the bands at 1038 cm^{-1} and 1188 cm^{-1} appear due to the vibrations of $-\text{SO}_3^-$ in Red 27 $\text{Zn}_2\text{Al-LDH}$. This indicates that intercalation in the interlayer space involves hydrogen bonding, besides the obvious electrostatic attraction between the electropositive cations in the layer and the organic anions in the interlayer.

The thermogravimetric analyses (TGA) are suitable for determining the thermal stability of the materials, and were thus used to investigate the thermal stabilities of Acid Red 27 and Red 27-LDH. The thermal stability of Acid Red 27 and Red 27-LDH are studied using the TGA analysis. The TGA curves are shown in Fig. 4 (a and b). In the case of Acid Red 27 (Fig. 4 a), there are four steps in the temperature ranges of $50\text{--}330\text{ }^\circ\text{C}$, $330\text{--}550\text{ }^\circ\text{C}$, $550\text{--}728\text{ }^\circ\text{C}$, and $728\text{--}810\text{ }^\circ\text{C}$, that are attributed to decomposition of the Red 27 anions. The mass loss value at $870.8\text{ }^\circ\text{C}$ of Acid Red 27 is 36.25%.

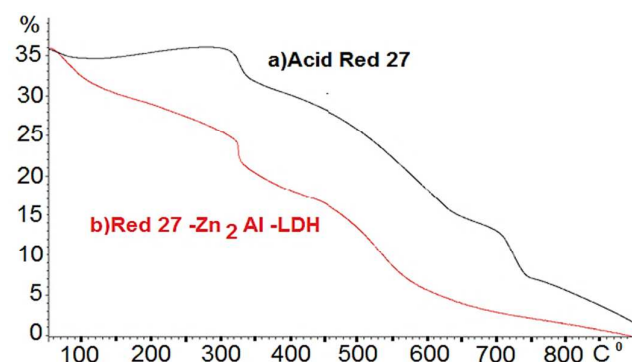


Fig. 4 TGA thermograms of (a) Acid Red 27 and (b) Red 27- Zn₂Al-LDH

Red 27-LDH shows major mass losses in three steps. The first mass loss observed in 120–325 °C corresponds to the loss of both adsorbed and interlayer water molecules. The following rapid mass loss in the region of 325–517 °C is attributable to decomposition of Red 27 and dehydroxylation of the LDH layer. The third mass loss in the temperature range of 517–718 °C is attributed to further dehydroxylation of the LDH layers. The mass loss value of Red 27-LDH at 872.04 °C is 38.14%. The comparison of the two thermogravimetric curves from Fig. 4 shows that Red 27- Zn₂Al-LDH has a lower percentage value of decomposition than Acid Red 27.

The scanning electron microscopy (SEM) image of the Red 27-LDH nanohybrid with two magnifications (a and b) is depicted in Fig. 5. The irregular bullet-like characteristic of the Red 27-LDH nanohybrid can be seen clearly in Fig. 5. In fact, Red 27-LDH is composed of aggregates of irregular semi-bullet-like nanoparticles with pellet thickness in the range of 32–34 nm. Broadening of the XRD pattern of Red 27-LDH (Fig. 2) is due to the nanosize of the particles.

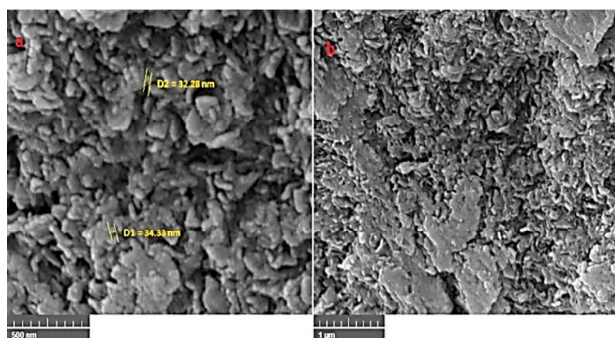


Fig. 5 SEM images of Red 27- Zn₂Al-LDH

The chemical composition of Al, Zn, O, C, N, and S in the Red 27- Zn₂Al-LDH nanohybrid at the microscopic level was analyzed by the energy dispersive X-ray spectroscopy (EDX). The EDX analysis (Fig. S2 in the Supporting Information) showed that Al, Zn, and O peaks were obviously found in the spectra which confirm the composition of LDH in presence of C, N, and S attributed to the Acid Red 27 molecules.

3.2 Photoluminescence behavior of Acid Red 27 and the Red 27- Zn₂Al-LDH nanohybrid

Photoluminescence usually involves a photoexcitation/emission process without an oxidation/reduction chemical reaction. Series of the fluorescence dye molecules intercalated in the LDH materials exhibited several new photophysical properties compared with those of the pristine dye systems.⁴⁶ Recently some researchers have reported that the emission spectrum of the fluorescence dye molecules intercalated into LDH exhibited a red or blue shift compared with that of a dilute solution.⁶⁷⁻⁶⁹ Furthermore, it was demonstrated that the luminescent properties and the molecule arrangement of the dyes can be tuned to some extent after intercalation into the LDH layer.⁷⁰ Generally, two types of aggregates of the dye molecule can be formed depending on the angle between the transition dipole and the lineation of the central vector of the two dye molecules. They are named *H-type* (face-to-face arrangement) and *J-type* (tail-to-tail arrangement) dimers, which are responsible for the blue and red shifts in the emission property of the dye molecules, respectively.

The photoluminescence (PL) behavior is correlated with the transference of the photo-induced electrons and holes, which can reveal the separation-recombination process of the photo-induced charge carriers. The PL emission spectra of the Red 27 Azo dye were studied in the excitation wavelengths of 260 nm and 220 nm, and those of Red 27-Zn₂Al-LDH were studied in the excitation wavelengths of 240 nm, 280 nm, and 360 nm at solid state (Fig. 6). The Acid Red 27 Azo dye shows the strongest PL emission peak at 569 nm and another one at 440 nm attributed to the excitation wavelength of 260 nm. The strong emission of Red 27- Zn₂Al-LDH at 542 nm and 436 nm attributed to the excitation wavelength of 240 nm, which is weaker than that of the Red 27 Azo and has smaller blue shift compared to the Red 27 Azo, indicates a low rate of electron-hole recombination in Red 27- Zn₂Al-LDH. This may be

favorable for the photocatalytic performance.⁷¹ Therefore, the blue-shift of the spectrum for the Red 27- Zn₂Al-LDH sample may be attributed to the formation of the H aggregate with π - π or dipole-dipole interaction and stabilization of Acid Red 27 molecules in the gallery of the LDH layer.

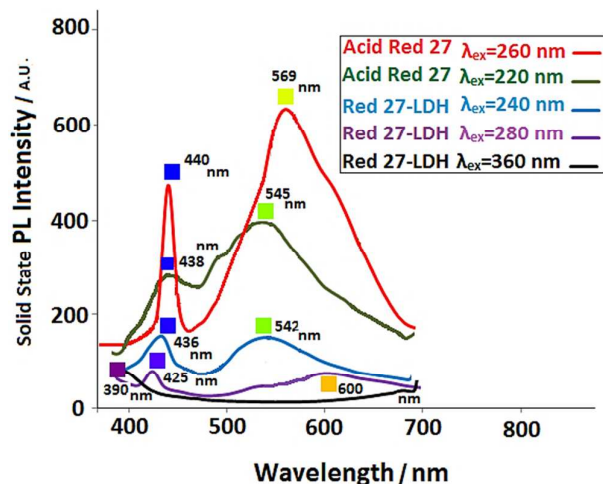


Fig. 6 Photoluminescence (PL) emission spectra of excitation wavelength at 260 nm and 220 nm of the Red 27 Azo dye, and excitation wavelength at 240 nm, 280 nm, and 360 nm of Red 27-Zn₂Al-LDH.

The Acid Red 27 molecule contains three sulfonate and one hydroxyl groups, which facilitate the direct intercalation to the LDH nanosheets based on both electrostatic and hydrogen-bond interactions. The resulting Red 27-Zn₂Al-LDH shows long range-ordered structures, which show blue-shift for the green luminescence. Additionally, the Red 27-Zn₂Al-LDH system with dual-color emission (green and blue, Fig. S3 in the Supporting Information) has been created, which shows changes in fluorescence of Acid Red 27.

As shown in Fig. 7, this kind of alignment (H-type) for the guest Red 27 anions in the spatial space of the LDH layers is confirmed by the micro structural analysis of the molecular dynamic (MD) calculation, which was indicated in the next molecular simulation section. Therefore, in this work, the blue-shift of the spectrum for the Red 27- Zn₂Al-LDH sample may be attributed to the formation of the H aggregate with π - π or dipole-dipole interaction in the gallery of the LDH layer. This phenomenon is also consistent with the horizontal arrangement of the Acid Red 27 anions with respect to the LDH layer as obtained from the XRD result. The two blue shifted wavelength emissions suggest that the intercalation of the

guest dye molecules within the layer matrix can stabilize the excited-state of the chromophores effectively. This can be attributed to the fact that the rigid and restricted space imposed by the LDH layers can conquer the thermal vibration and rotation of the guest Red 27 anions due to the non-radiative relaxation process in their excited states.⁴⁶ Since the molecular dynamic investigation can be used for calculation of the host-guest electrostatic interaction, hydrogen bonding, stability, and diffusion study of the intercalated molecules in the LDH layers, it is preferred to the first principle study by quantum mechanics (QM) calculation. Also the QM study of the ideal supercell with over 100 atoms, as we have reported in the previous work,⁷² is very expensive for the LDHs with large azo molecules. In fact the molecular dynamic simulation after molecular modeling not only can predict the calculated X-ray diffraction (XRD) pattern for the synthesized LDHs materials, but can also offer layer by layer aggregation with the π - π or dipole-dipole interaction in the gallery of the LDH layer.

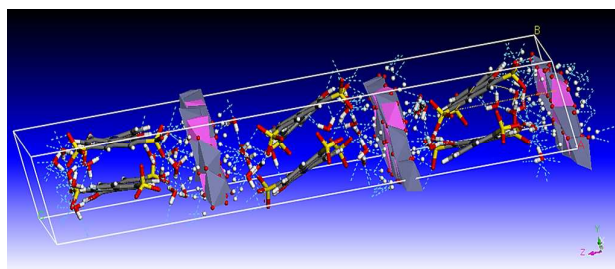


Fig. 7 H type (side by side) arrangement of the Acid Red 27 molecules with π - π interaction of the adjacent azo molecules by the structural optimization using the molecular dynamic simulation

As shown in Fig. 2, the (003) diffraction peak of the intercalation compound moves to the low angle region compared to Zn₂Al-NO₃-LDHs. The sharp peaks of (003), (006), and (009) present good multiple relationships and indicate that the crystalline layered structure was held in the whole intercalation range. Therefore, it can be concluded that the Acid Red 27 molecules were intercalated successfully which implies that the crystallites are orderly stacked in the *c* direction and the intercalated Acid Red 27 molecules are orientated in an orderly fashion within the interlayer space due to the strong π - π aggregation⁷³ effect of the Acid Red 27 molecules. As shown in Fig. 9, good agreement between the calculated and experimental d_{003} confirms the appropriate intercalation of the Acid Red 27 molecules in Zn₂Al-LDHs. Also as presented in Fig. 7, the

MD simulation study shows that the Acid Red 27 molecules adopt a preferred almost inclined face-to-face arrangement of the adjacent Acid Red 27 molecules and the acidic groups are parallel to the LDH layers which are responsible for the enhanced polarization of the photoemission behavior of the hybrid LDHs. Moreover, it can be expected that using the co-aggregation process described here, numerous anionic species are assembled into the LDH layers for designing and fabricating the organic-inorganic functional materials based on the synergetic relationship between the organic anions and the small cation.⁷⁴ Therefore, this work provides a simple method for the construction of LDHs with one-/two-color luminescence by incorporation of the photoactive anions within a two-dimensional LDH inorganic matrix, which can also be applied as the stabilized luminescent materials.⁷⁵

3.3 Optical Property of Acid Red 27 and the Red 27- Zn₂Al-LDH nanohybrid

In Fig. 8 a, the diffuse reflectance spectroscopy (DRS) of Red 27- Zn₂Al-LDH indicates that the absorbance spectrum as an increased broad absorbance area ranges approximately from 300 to 680 nm after intercalation of Acid Red 27 into LDHs. The red shift of the absorbance edge led us to conclude that there was a well-ordered host-guest interaction due to the charge transfer of the azo dye carboxylate group to the metals of the LDH layer. This confirms the photocatalytic capability of Red 27- Zn₂Al-LDH and the existence of the aggregation-improved luminescence.⁷⁶ The optical band gap energy, E_g , of Red 27- Zn₂Al-LDH was determined by UV-vis- DRS and the obtained DRS spectrum is reported by the Kubelka-Munk function.^{77,78}

Determination of E_g for the sample was done using the Kubelka-Munk (K-M) Eq. (1):

$$\alpha = \frac{(1-R)^2}{2R} \quad (1)$$

where R is the reflectance and α is the Kubelka-Munk function. The experimental value of the band gap energy calculated for Red 27- Zn₂Al-LDH is $E_g=2.5$ eV, which is presented in Fig. 8 b. These results show that Acid Red 27 molecules with sulfonate head groups have remarkable red shift and broad area absorbance edge when intercalated into the Zn-Al-LDH matrix in comparison with the

pristine Acid Red 27. The results also show decrease in the band gap energy in comparison with Zn-Al-NO₃-LDH⁷⁹ as the LDHs contain small anions. So the Acid Red 27 molecules can have band gap energy lower than that of the luxurious photocatalytic materials such as TiO₂ (3.23 eV), ZnO(3.21 eV), ZnS(3.60 eV), and α -Fe₂O₃(3.1 eV).^{80,81}

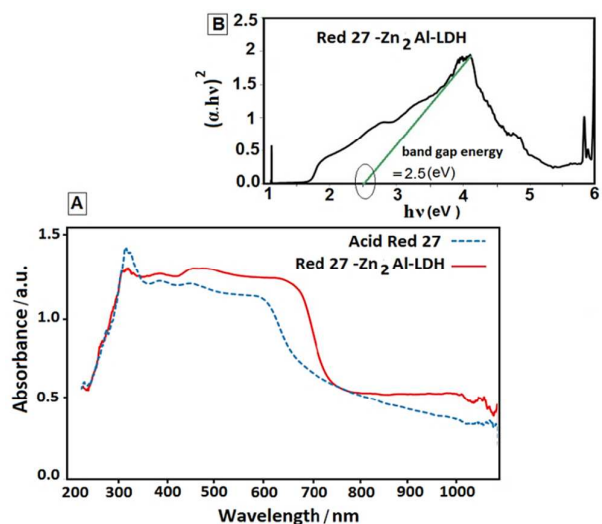


Fig. 8 A) DRS-UV-visible absorption spectrum of Red 27- Zn₂Al-LDH and Acid Red 27 and B) Kubelka-Munk transformed reflectance spectrum for Red 27- Zn₂Al-LDH

3.4 Results of the molecular modeling and simulation

The orientation of the Red 27 anions within the interlayer space depends on the space available for the guest anions in the interlayer region. On the basis of the d_{003} value of Red 27-LDH (measured by the x-ray diffraction), the space available for the Red 27 anions in the interlayer space is 12.18 Å, which can be calculated by subtracting the layer thickness of 4.8 Å from the interlayer space (16.98 Å). According to the longitudinal van der Waals radius of the Red 27 anion (9.84 Å), enough vacant space is available for horizontal intercalation of the guest anions. On the other hand, the orientation of the guest anions depends on the interactions of the guest anions with the LDH layers, the interlayer water molecules, and also the interaction of the guest-guest anions. The experimental XRD results combined with the molecular simulations can determine the potential orientations of the Red 27 guest anions in the interlayer space. The water content of the interlayer space,

the position of the interlayer water molecules, and also the orientation of the guest anions (Red 27) strongly influence the x-ray diffraction patterns. By the molecular modeling and minimization, the water molecules and guest anions arranged within the interlayer; so that the calculated XRD pattern agrees with the measured one. Fig. 9 shows the calculated and experimental XRD patterns of Red 27-LDH. The experimental XRD pattern shows that the peak maxima of d_{003} , d_{006} , and d_{009} were observed at 16.98, 8.63, and 5.79 Å, respectively, while the calculated XRD pattern shows them at 16.98, 8.49, and 5.67 Å, respectively. Note the particularly good agreement between the calculated and experimental d_{003} .

In our previous work,⁵¹ intensities of the experimentally determined (003) and (006) peaks were inverted compared to those in the calculated XRD pattern. But in the present work, Good agreement between the experimental diffraction pattern and the calculated XRD shows that the surface of Red 27-Zn₂Al-LDH is regular and the (003) reflection intensity is higher than that of (006) in the experimental XRD pattern as expected. The slightly higher value for the experimental d_{006} spacing compared to that of the calculated d_{006} may be related to the effect of the crystal size on the peak broadening as well as to the high disorder of the guests in the structural model, which is not taken into account in the software.⁸² The XRD anisotropic peak broadening due to the non-spherical and nano-crystallite structure of Red 27-LDH, residual stress, defects in the crystal structure, and finally the equipment reason, are the other factors that can deform the lattice, which causes peak shift. These are fairly typical in the solid solutions.

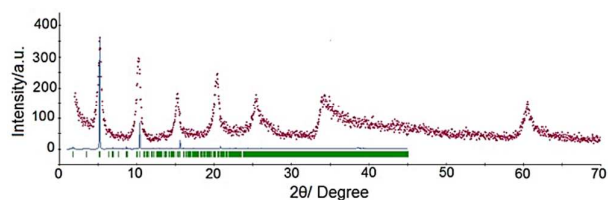


Fig. 9 The calculated and experimental X-ray diffraction patterns, blue peak: calculated XRD, dotted red peak: experimental XRD

The *aggregation* state of the structure at the microscopic level is a very important factor in determining the macroscopic activities of the Acid Red 27 molecules intercalated into the layers of LDH such as the photoluminescence property. The MD simulation (Fig. S4 in

the Supporting Information) shows positioning of the intercalated molecules at the molecular level which leads to the determination of the arrangement of the guest Acid Red 27 molecules with face to face or coplanar conformation in the interlayer region. Also Fig. 10 (a and b) shows a snapshot of the equilibrium structures of the Red 27 LDH system before and after the MD simulation. Note that prior to simulation, the Acid Red 27 molecules and water molecules were placed randomly in the interlayer space of LDH. Through analyzing the trajectories, the equilibration of the simulation systems reveals the arrangement of the Red 27 anions. The molecular dynamic calculations (Fig. S7 in the Supporting Information) reveal that the long axis of the Acid Red 27 molecules in the interlayer space displays approximately 78° tilt from the perpendicular orientation to the LDH layer. These calculations also show that the guest anions are not randomly distributed in the interlayer space, but they have tendency to assemble in rows, although there is a certain level of disorder.⁵¹

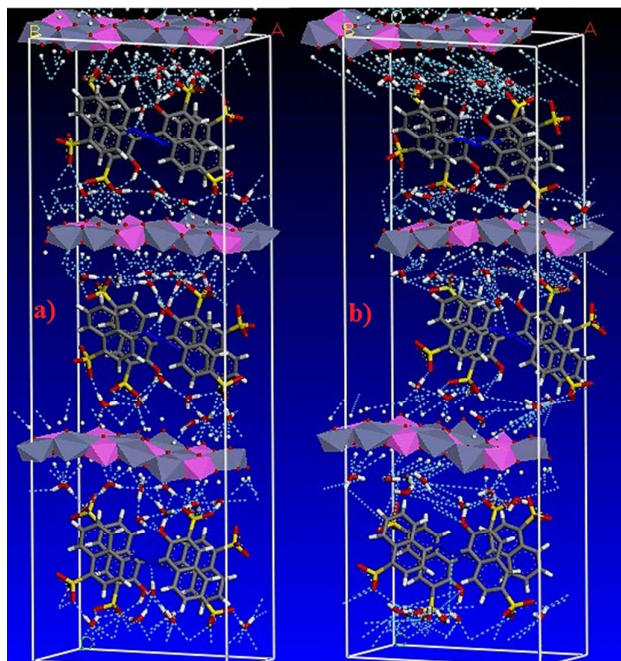


Fig. 10 Snapshot of the Equilibrium structures for Red 27-Zn₂Al-LDH, (a) before and (b) after the MD simulation

To characterize the orientation of the Acid Red 27 molecules at the interface of the LDH layers, the *angle distribution* was analyzed from the trajectory file of the molecular dynamic simulation of Red 27-Zn₂Al-LDH. The orientation of the Red 27 anion tail vectors was calculated with respect to the perpendicular direction (i.e. z axis) to

the plane of the interface (xy plane). The vector connecting the N atom and the terminal S atom is defined as the tail vector. Fig. S7 in the supporting information shows the tilt angle (θ) between the tail vector and the vector that is normal to the layer surface in the Red 27-LDH systems. Fig. S5 in the Supporting Information displays the mode of the Acid Red 27 molecules in the interlayer space. The tail of Acid Red 27 is slanted to the LDH layers. The tail vector of the Acid Red 27 molecules is tilted with an average tilt angle from 73° to 82° . We can see from Fig. S5 that the most of the tilt angles are about 78° . The end-group water interaction can be attained from the *partial radial distribution functions* (RDFs) which explain how many atoms of type A are on average at the r distance of an atom of type B.⁵⁷ The relevant RDF of the water molecules to the Acid Red 27 molecules end-group are calculated over the last 2000 ps (Fig. S6 in the supporting information). As can be seen in Fig. S6, the water molecules are dispersed in the interlayers of LDH around the head groups, and can be divided into two main shells which are placed around 0.99 Å and 1.41 Å to the Acid Red 27 molecules' end-group respectively. Most of the water molecules have close contact with OH^- of the LDH layer and the SO_3^- group of the guest anions. Fig. S7 and Fig. S4 indicate the scheme of the H-bond structure between the end-group and the water molecules which shows that most of the hydrogen bonds in the hybrid systems are developed by the O atom of the end-groups between OH^- in the layers of LDH and the water molecules.

To study the stability, immobilization, and effective delivery of the Acid Red 27 molecules which use LDH as the carriers, we have obtained the *mean square displacements* (MSDs) of Acid Red 27 and the water molecules from the last 2000 ps (time step equal to 0.4 fs and total time of simulation equal to 2000ps) MD trajectory. The analysis of MSD yields important information about the stability of the Red 27-LDH system. The slopes of the MSD-versus-time curves are consistent with the system-achieving equilibrium. The MSD of the two different molecules in 2000 ps of trajectory is shown in Fig. 11. The MSD was obtained from Eq. (1):⁵⁰

$$\text{MSD}(t) = \frac{1}{N} \left[\sum_{i=1}^N [\mathbf{r}_i(t) - \mathbf{r}_i(0)]^2 \right] \quad (1)$$

where N is the number of the target molecules and $\mathbf{r}_i(t)$ is the location of the molecule i at time t . Then the diffusion coefficient (D) can be obtained using the famous Einstein relation, Eq. (2):⁸³

$$D\alpha = \frac{1}{2dN\alpha} \lim_{t \rightarrow \infty} \frac{d}{dt} \langle [\mathbf{r}_i(t) - \mathbf{r}_i(0)]^2 \rangle \quad (2)$$

where d is the system dimensionality and $\mathbf{r}_i(t)$ and $\mathbf{r}_i(0)$ are the centers of the mass coordinates of the i th Acid Red 27 and water molecules at the times t and $t=0$, respectively. Once MSD is calculated as the function of time, you are ready to calculate the self-diffusion coefficient. Eq.1 suggests that MSD exhibits linear dependence on time, and *self-diffusion coefficient* is just the slope of the line. For short times, the MSD dependency on time is clearly not linear, and it becomes linear just for longer times. The diffusion coefficient should be determined using only the data in the region where MSD depends linearly on time, and by using linear regression.⁸⁴ Malfreyt et al.⁸⁵ have reported molecular dynamics simulation of Zn_2AlCl Layered Double Hydroxide. The mean-squared displacement was calculated using a trajectory of 500 ps and the results show that MSD is linear with the time (300 ps) for water molecules and they are confined in a small interlayer space. Also Yuan et al.⁵⁰ have calculated the mean square displacements (MSDs) of methyl orange (MO) and water molecules in interlayer space of $\text{Mg}_2\text{Al-LDH}$ from the last 1000 ps (1 ns) molecular dynamic (MD) trajectory. But the results show that MSD is not absolutely linear with time (500 ps) for water molecules. In our work, Fig. 11 shows the gained MSD for the intercalated water molecules in comparison with the obtained MSD for the molecule of Acid Red 27. And the MD trajectory for the intercalated water molecules from the last 2000 ps shows that MSD is not completely linear. Consequently, the water molecules have enough space in comparison with dye molecules in the interlayer space of $\text{Zn}_2\text{Al-LDH}$. According to the MSD curves, the self-diffusion coefficients of water and Acid Red 27 were calculated to be $(2.83 \pm 0.05) \times 10^{-8} \text{ cm}^2/\text{s}$ and $1.38 \pm 0.05 \times 10^{-8} \text{ cm}^2/\text{s}$ respectively. Based on this result, the self-diffusion coefficient of Acid Red 27 is lower than that of the water molecule. From the above mentioned analysis, it can be concluded that the Acid Red 27 molecules are restricted in the layers of LDH and the molecules of Acid Red 27 are stable when intercalated into the layers of LDH. The stability is highly important since it can overcome the thermal instability when Acid Red 27 is used alone.

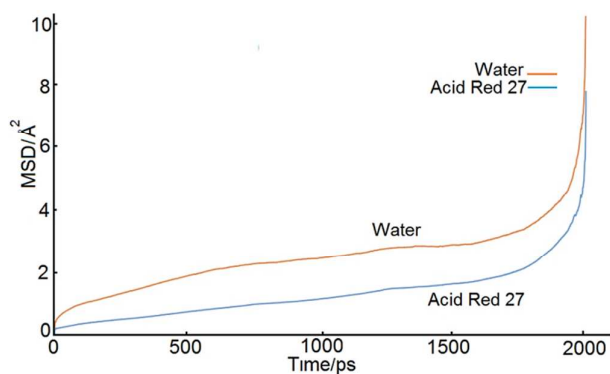


Fig. 11 Comparison of the calculated MSD for Acid Red 27 and the water molecules

Consequently molecular dynamics (MD) simulation reveals that the Red 27-Zn₂Al-LDH system exhibits ordered superlattice structure, which is in agreement with the experimental results. Therefore, this work affords a facile approach for the design and fabrication of organic-inorganic luminescent materials⁸⁶ with improved optical property.

Conclusions

In the present research, the synthesis and characterization of the Zn-Al hydrotalcite intercalated with the Acid Red 27 molecules were reported. Successful intercalation of the Acid Red 27 molecules into the interlayer space of LDH was confirmed by powder X-ray diffraction, FTIR spectroscopy, and thermal gravimetric analysis (TGA). Nano size and the chemical composition of Red 27-LDH were well characterized by scanning electron microscopy (SEM) and energy dispersive X-ray spectroscopy (EDX). During intercalation of the Red 27 anions, the layers of LDH swell to host the anions and this expansion is reflected by the value of d_{003} . The photoluminescence (PL) analysis indicated that Red 27-Zn₂Al-LDHs has two blue shifted wavelength emissions to guest pristine Acid Red 27. Also, the molecular dynamic simulation led to the investigation of the structural and dynamic properties of Red 27-LDH with ordered superlattice structure, which is in agreement with the experimental results. These results suggest that the *H-type* (face-to-face arrangement) aggregation of the Acid Red 27 molecules in the space of LDH interlayers improves the fluorescent property of Acid Red 27. The RDFs between the end-group of Acid Red 27 and water molecules showed that the hydrogen bonds in the hybrid system are developed by the O atoms of the end-groups between OH⁻ in the layers of LDH and the water molecules.

Finally the mean square displacement (MSD) analysis was obtained using the trajectory files according to the MD simulations which indicated that the Acid Red 27 molecules were more stable when intercalated into the layers of LDH.

Notes and references

- 1 M.S.Yen, I.J.Wang, *Dyes Pigments*, 2005, **67**, 183-188.
- 2 O. Varnavski, R.G. Ispasoiu, M. Narewal, J. Fugaro, Y. Jin, H. Pass, T. Goodson, *Macromolecule*, 2000, **33**, 4061-4068.
- 3 T.J. Dines and H. Onoh, *Spectrochim. Acta A.*, 2006, **64**, 891-900.
- 4 E. Vogel, A. Gbureck, W. Kiefer, *Journal of Molecular Structure*, 2000, **550**, 177-190.
- 5 H.S Nalwa, S. Miyata, CRC Press, New York, 1997.
- 6 G.J Lee, D.H. Kim, M.Y. Lee, *Appl. Opt.*, 1995, **34**, 138-143.
- 7 N .Biswas, S. Umapathy, *J. Phys. Chem.*, 2000, **104**, 2734-2745.
- 8 H.S. Rosenkranz, G. Klopman, *Mutagenesis.*, 1990, **5**, 137-146.
- 9 M.R. Fuh, K.J. Chia, *Talanta*, 2002, **56**, 663-671.
- 10 L.F. Capitan-Vallvey, M.D, Fernandez, *Talanta*, 1998, **47**, 861-868.
- 11 Y. Tian, G. Wang, F. Li, D.G. Evans, *Journal of Physics and Chemistry of Solids.*, 2007, **61**,1662-1666.
- 12 P. Tang, X. Xu, Y. Lin, D. Li, *Industrial & Engineering Chemistry Research.*, 2008,**47** ,2478-2483.
- 13 S. Guo, D.G. Evans, D. Li, *Journal of Physics and Chemistry of Solids.*, 2006, **67**,1002-1006.
- 14 S. Guo, D. Li, W. Zhang, M. Pu, D.G. Evans, X. Duan, *Journal of Solid State Chemistry.*, 2004,**177**, 4597-4604.
- 15 C. Taviot-Gueho, A. Illaïk, C. Vuillermoz, S. Commereuc, V. Verney, F. Leroux, *Journal of Physics and Chemistry of Solids.*, 2007, **68**,1140-1146.
- 16 K. Parida, L. Mohapatra, *Chemical engineering journal.*, 2012, **179**, 131-139.
- 17 (a) S. P. Newman and W. Jones, *New J. Chem.*, 1998, **22**, 105-115; (b) V.Rives, Layered Double Hydroxides: Present and Future, *Nova Sci. Pub. Co, Inc.*, New York 2001, **4**, 1-115.
- 18 (a) A. I. Khan and D. O'Hare, *J. Mater. Chem.*, 2002, **12**, 3191-3198; (b) F. Leroux and C. Taviot-Gueho, *J. Mater. Chem.*, 2005, **15**, 3628-3642.
- 19 H. Zhang, Z. P. Xu, G.Q. Lu, and S. C. Smith, *Phys. Chem. C*, 2009, **113**, 559-566.

Journal Name

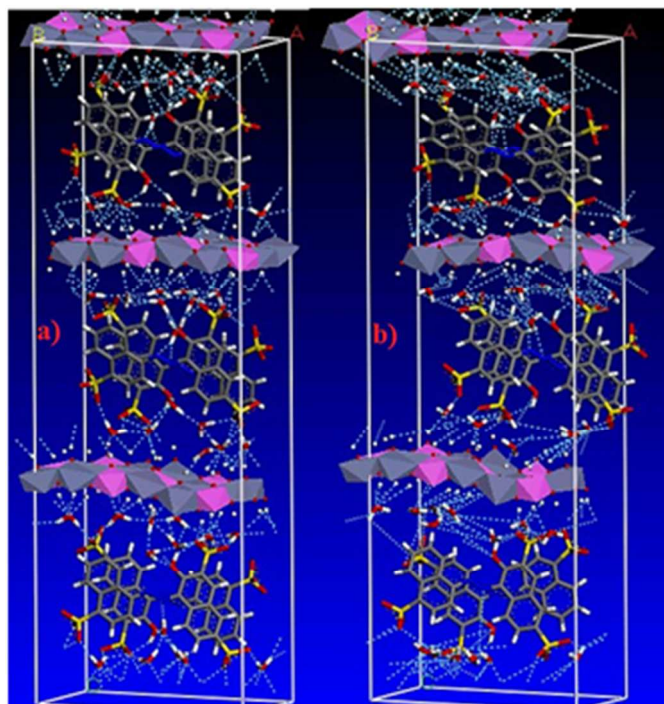
ARTICLE

- 20 M.Q. Zhao, Q. Zhang, J.-Q. Huang and F. Wei, *Adv. Funct. Mater.*, 2012, **22**, 675-694.
- 21 Q. Wang and D. O'Hare, *Chem. Rev.*, 2012, **112**, 4124-4155.
- 22 F. Geng, R. Ma and T. Sasaki, *Acc. Chem. Res.*, 2010, **43**, 1177 - 1185.
- 23 M. Shao, J. Han, M. Wei, D. G. Evans and X. Duan, *Chem. Eng. J.*, 2011, **168**, 519-524.
- 24 Y. Zhao, M. Wei, J. Lu, Z. L. Wang and X. Duan, *ACS Nano*, 2009, **3**, 4009-4016.
- 25 C. Gomes Silva, Y. Bouzidi, V. Fornes and H. Garcia, *J. Am. Chem. Soc.*, 2009, **131**, 13833-13839.
- 26 L. Teruel, Y. Bouzidi, P. Atienzar, V. Fornes and H. Garcia, *Energy Environ. Sci.*, 2010, **3**, 154-159.
- 27 Y. Zhao, S. He, M. Wei, D. G. Evans and X. Duan, *Chem. Commun.*, 2010, **46**, 3031-3033.
- 28 Q. Wang, H. H. Tay, Z. Zhong, J. Luo and A. Borgna, *Energy Environ. Sci.*, 2012, **5**, 7526-7530.
- 29 Q. Wang, J. Luo, Z. Zhong and A. Borgna, *Energy Environ. Sci.*, 2011, **4**, 42-55.
- 30 D. G. Evans and X. Duan, *Chem. Commun.*, 2006, **6**, 485-496.
- 31 J. Han, Y. Dou, J. Zhao, M. Wei, D. G. Evans and X. Duan, *Small*, 2013, **9**, 98-106.
- 32 C. Forano, T. Hibino, F. Leroux, C. Taviot-Gueho, F. Bergaya, B. K.G. Theng, G. Lagaly, *Handbook of clay science*, Elsevier, Amsterdam, 2006, **1**, 1021-1095.
- 33 F. Kovanda, K. Jiratova, R. Kalouskova, F.L. Gerard, *Nova Sci.*, 2006, **1**, 89-139.
- 34 F. Li, X. Duan, D.G. Evans, *Layered Double Hydroxides*, Springer, Berlin/Heidelberg., 2006, **119**, 193-223.
- 35 (a) G. Ihlein, F. Schuth, O. Krauu, U. Vietze and F. Laeri, *Adv. Mater.*, 1998, **10**, 1117-1119; (b) B. J. Scott, G. Wirnsberger, M. D. McGehee, B. F. Chmelka and G. D. Stucky, *Adv. Mater.*, 2001, **13**, 1231-1234; (c) G. Calzaferri, S. Huber, H. Maas and C. Minkowski, *Angew. Chem., Int. Ed.*, 2003, **42**, 3732- 3758; (d) M. Busby, A. Devaux, C. Blum, V. Subramaniam, G. Calzaferri and L. De Cola, *J. Phys. Chem. C*, 2011, **115**, 5974-5988; (e) C. A. Strassert, C.-H. Chien, M. D. G. Lopez, D. Kourkoulos, D. Hertel, K. Meerholz and L. De Cola, *Angew. Chem., Int. Ed.*, 2011, **50**, 946-950.
- 36 (a) C. M. Carbonaro, A. Anedda, S. Grandi and A. Magistris, *J. Phys. Chem. B*, 2006, **110**, 12932-12937; (b) I. Garcia-Moreno, A. Costela, A. Cuesta, O. Garcia, D. del Agua and R. Sastre, *J. Phys. Chem. B*, 2005, **109**, 21618-21626; (c) D. P. Yan, G. O. Lloyd, A. Delori, W. Jones and X. Duan, *ChemPlusChem*, 2012, **77**, 1112-1118.
- 37 M. Ogawa and K. Kuroda, *Chem. Rev.*, 1995, **95**, 399-438.
- 38 W. Guan, J. Lu, W. Zhou and C. Lu, *Chem. Commun.*, 2014, **50**, 11895-11898.
- 39 (a) D. P. Yan, J. Lu, M. Wei, J. B. Han, J. Ma, F. Li, D. G. Evans and X. Duan, *Angew. Chem., Int. Ed.*, 2009, **48**, 3073-3076; (b) D. P. Yan, J. Lu, J. Ma, M. Wei, D. G. Evans and X. Duan, *Angew. Chem., Int. Ed.*, 2011, **50**, 720-723; (c) Z. Li, J. Lu, S. D. Li, S. H. Qin and Y. M. Qin, *Adv. Mater.*, 2012, **24**, 6053-6057.
- 40 D. Yan, M. Wei, Layered Double Hydroxide Materials: Assembly and Photofunctionality." *Photofunctional Layered Materials*. Springer International Publishing, 2015, **166**, 1-68.
- 41 W. Li, D. Yan, R. Gao, J. Lu, M. Wei, and X. Duan, *Journal of Nanomaterials*, 2012, **2013**, 1-14
- 42 Y. Zhao, H. Lin, M. Chen, and D. Yan, *Ind. Eng. Chem., Res.* 2014, **53**, 3140-3147.
- 43 R. Gao, M. Zhao, Y. Guan, X. Fang, X. Li and D. Yan, *J. Mater. Chem. C*, 2014, **2**, 9579-9586.
- R. Gao, X. Lei, M. Chen, D. Yan. and M. Wei, *New J. Chem.*, 2013, **37**, 4110-4118.
- 45 G. Wang, S. Xu, C. Xia, D. Yan, Y. Lin and M. Wei, *RSC Adv.*, 2015, **5**, 23708-23714.
- 46 C. Li, D. Yan, M. Wei, *Sensors and Actuators B* ., 2015, **216** , 198-203.
- 47 S.P. Newman, T.D. Cristina, P.V. Coveney, *Langmuir.*, 2002, **18** ,2933-2939.
- 48 E. Kafunkova, C. Taviot-Gueho, P. Bezdiccka, M. Klementova, P. Kovar, P. Kubat, J. Mosinger, M. Pospisil, K. Lang, *Chem. Mater.*, 2010, **22** ,2481-2490.
- 49 D.P. Yan, J. Lu, M. Wei, D.G. Evans, X. Duan, *J. Mater. Chem.*, 2011, **21**, 13128-13139.
- 50 K. Lv, H. Kang, H. Zhang and S. Yuan, *Colloids .Surf., A*, 2012, **402**, 108-116.
- 51 Z. Rezvani, F. Arjomandi Rad and F. Khodam, *Dalton Trans.*, 2015, **44**, 988-996.
- 52 Discover, User Guide, Accelrys, *Molecular Simulations Inc*, San Diego, USA., 1996.
- 53 S. P. Newman, S. J. Williams, P. V. Coveney, W. J. Jones, *Phys. Chem. B*, 1998, **102**, 6710-6719. (b) S. P. Newman, H. C. Greenwell, P. V. Coveney, W. Jones, *Layered Double Hydroxides: Present and Future*; Nova Science, New York, USA, 2001.
- 54 R.P. Iozano, C. Rossi, A.L. Iglesia, and E. Matesanz, *American Mineralogist.*, 2012, **97**, 513-523.

ARTICLE

Journal Name

- 55 W.D. Cornell, P. Cieplak, C.I. Bayly, I.R. Gould, K.M. Merz, D.M. Ferguson, D.C. Spellmeyer, T. Fox, J.W. Caldwell, P.A. Kollman, *J. Am. Chem. Soc.*, 1995, **117**, 5179-5197.
- 56 N. Karasawa, W.A. Goddard, *J. Phys. Chem.*, 1989, **93**, 7320-7327.
- 57 J.E. Lennard-Jones, *On the Forces between Atoms and Ions*, Proc.R. Soc. Lond., A, 1925, **109**, 584-597.
- 58 P. Kustrowski, D. Sulkowska, L. Chmielarz, A. Rafalska-Lasocha, B. Dudek, and R. Dziembaj, *Microporous Mesoporous Mater.*, 2005, **78**, 11-22.
- 59 C. Li, G. Wang, D.G. Evans, and X. Duan, *J. Solid State. Chem.*, 2004, **177**, 4569-4575.
- 60 J.T. Klopprogge, L. Hickey, and J.L. Frost, *Appl. Clay Sci.*, 2001, **18**, 37-49.
- 61 M. Wei, X. Xu, J. He, Q. Yuan, G. Rao, D.G. Evans, M. Pu, and L. Yang, *J. Phys. Chem. Solids.*, 2006, **67**, 1469-1476.
- 62 F. Cavani, F. Trifiro, and A. Vaccari, *Catal.Today*. 1991, **11**, 173-301.
- 63 K. Nakamoto, *Infrared and Raman Spectra of Inorganic and Coordination Compounds, Part B, Applications in Coordination, Organometallic, and Bioinorganic Chemistry*, Wiley, New York, 5th edn, 1997.
- 64 S.J. Santosa, E. S. Kunarti, and E. Karmanto, *Appl. Surf. Sci.*, 2008, **254**, 7612-7617.
- 65 H. Gunzler and H.U. Gremlich, *IR Spectroscopy: An Introduction*, Wiley-VCH, Weinheim, New York, 2002.
- 66 M. Asniza, A.M. Issam and H.P.S. Abdul Khalil, *Sains Malaysiana*, 2011, **40**, 765-770.
- 67 E. Kafunkova, C. Taviot-Gueho, P. Bezdicka, M. Klementova, P. Kovar, P. Kubat, J. Mosinger, M. Pospsil, K. Lang, *Chem. Mater.* 2010, **22**, 2481-2490.
- 68 M. Jirickova, J. Demel, P. Kubat, J. Hostomsky, F. Kovanda, K. Lang, *J. Phys. Chem. C*, 2011, **115**, 21700-21706.
- 69 U. Costantino, N. Coletti, M. Nocchetti, G. G. Aloisi and F. Elisei, *Langmuir*, 1999, **15**, 4454-4460.
- 70 D. P. Yan, J. Lu, J. Ma, S. Qin, M. Wei, D. G. Evans and X. Duan, *Angew. Chem., Int. Ed.*, 2011, **50**, 7037-7040.
- 71 Y. Zhao, B. Li, Q. Wang, W. Gao, C. J. Wang, M. Wei, D. G. Evans, X. Duan and D. O'Hare, *Chem. Sci.*, 2014, **5**, 951-958.
- 72 F. Arjomandi Rad and Z. Rezvani, *RSC Adv.*, 2015, **5**, 67384-67393.
- 73 S. Zheng, J. Lu, W. Li, Y. Qin, D. Yan, D.G. Evans, X. Duan, *J. Mater. Chem. C*. 2014, **2**, 5161-5167.
- 74 D. Yan, J. Lu, L. Chen, S. Qin, J. Ma, M. Wei, D. G. Evans, X. Duan, *Chem. Commun.* 2010, **46**, 5912-5914.
- 75 H. Ma, R. Gao, D. Yan, J. Zhao, M. Wei, *J. Mater. Chem. C*. 2013, **1**, 4128-4137.
- 76 T. Shen, Y. Zhang, W. Liu, Yu Tang, *J. Mater. Chem. C*. 2015, **3**, 1807-1816.
- 77 H.M. ali, M.M. Abou-Mesalam, and M.M. El-Shorbagy, *J. Phys. Chem. Solids.*, 2010, **71**, 51-55.
- 78 K.H. Reddy, S. Martha, and K.M. Parida, *Inorganic Chemistry.*, 2013, **52**, 6390-6401.
- 79 Chai, X. Xu, Y. Lin, D.G. Evans and D. Li, *Polym. Degrad. Stab.*, 2009, **94**, 744-749.
- 80 M.R. Hoffmann, S.T. Martin, W.Y. Choi and D.W. Bahnemann, *Chem. Rev.*, 1995, **95**, 69-96.
- 81 A.V. Emeline, G.V. Kataeva, V.K. Ryabchuk and N. Serpone, *J. Phys. Chem. B*, 1999, **103**, 9190-9199.
- 82 P. Kovar, K. Melanova, V. Zima, L. Benes, P. Capkova, *J. Colloid Interface Sci.* 2008, **319**, 19-24.
- 83 M.P. Allen and D.J. Tildesley, *Computer Simulation of Liquid*, Oxford Science Publications, Oxford, 1987.
- 84 D. Frenkel, B. Smit. *Understanding Molecular Simulation: From Algorithms to Applications*, Academic Press, San Diego, 2th edn, 2002.
- 85 J. Pissou, J. P. Morel, N. Morel-Desrosiers, C. Taviot-Gueho, and P. Malfreyt, *J. Phys. Chem. B*, 2008, **112**, 7856-7864.
- 86 R. Liang, S. Xu, D. Yan, W. Shi, R. Tian, H. Yan, M. Wei, David G. Evans, and X. Duan, *Adv. Funct. Mater.* 2012, **22**, 4940-4948.



Graphical Abstract
71x74mm (120 x 120 DPI)